Typhoon risk and climate-change impact assessment for cultural heritage asset roofs

Giacomo Sevieri[1,*] , Carmine Galasso[2]

[1]*Research Fellow, Ph.D., Department of Civil, Environmental and Geomatic Engineering, University College London, Gower Street, London, WC1E 6BT, United Kingdom. E-mail: g.sevieri@ucl.ac.uk*

[2]*Associate Professor, Ph.D., Department of Civil, Environmental and Geomatic Engineering, University College London, Gower Street, London, WC1E 6BT, United Kingdom; and Scuola Universitaria Superiore (IUSS) Pavia, Piazza della Vittoria 15, Pavia, 27100, Italy. E-mail: c.galasso@ucl.ac.uk*

Abstract

Recent catastrophic events in Southeast Asia have emphasized that roofs made of wood/steel frames and lightweight metal roofing sheets are the most vulnerable component in the building envelope when subjected to typhoon-induced wind uplift. This also applies to ageing cultural heritage (CH) assets, which deserve special consideration because of their intangible value for local communities, and their essential role for inclusive and sustainable socio-economic development through cultural tourism.

This paper introduces a simulation-based framework for fragility derivation and typhoon risk assessment of CH-asset roofs. Fastener pullout and roof-panel pullover are explicitly considered in the proposed framework to model the progressive failure of the roof system. A simplified roof geometry is assumed, requiring limited information about the structure under investigation and low computational resources. Such a low computational burden allows one to model wind-induced demands and component capacities probabilistically as well as to consider the effects of load redistributions due to fastener failure and fastener/roof-panel corrosion. Variance-based sensitivity

* Corresponding author. Tel.: +39 349 2138290; e-mail address: g.sevieri@ucl.ac.uk (G. Sevieri).

analysis (i.e., Sobol’ indices) based on polynomial chaos expansions of the limit state function is also performed, highlighting the parameters most affecting typhoon-risk variance and then requiring special attention during data collection. Climate-change impact on the typhoon risk estimates is finally investigated through the use of various scenarios and a time-dependent function modifying the wind hazard profile of the site where the assets of interest are located.

The proposed framework is applied to 25 CH assets in Iloilo City, Philippines. The required input data was collected through rapid visual surveying combined with new technologies, such as drones. It is shown that the proposed framework can be adopted in practice for both risk prioritization at a building-portfolio level and simplified risk assessment at a building-specific level.

Keywords

Typhoon risk assessment; Typhoon risk prioritization; Cultural Heritage; Climate Change, Sobol’ indices

1. Introduction and Motivation

Developing countries are disproportionately affected by natural hazards and lack coping capacities. This combination sets back progress on poverty alleviation and slows long-term development (Strobl, 2019). In this context, probabilistic catastrophe risk models - estimating potential human and economic losses due to natural hazards - are essential tools for robust and effective pre-disaster preparedness and financial planning to reduce disaster risk and enhance societal resilience. Risk modeling for developing countries emphasizes specific challenges in terms of quantity and quality of the available input data; widening the types of considered hazards and structures/infrastructure and ensuring models are contextualized to local needs is also crucial.

This paper focuses explicitly on typhoon risk and climate-change impact assessment for cultural heritage (CH) assets in developing countries. CH assets are highly exposed and vulnerable to natural hazards and resource management, conflict, climate change, and a host of other factors. CH assets require special consideration because of their symbolic value for a given community and their links with local economies, for instance, by attracting investment and promoting green, locally-based, and stable jobs related to a wide range of sustainable activities in areas such as tourism, conservation, construction, and art in general. In fact, cultural tourism is one of the priority sectors by which many governments in developing countries aim to foster inclusive and sustainable socio-economic development.

Post-event surveys worldwide have highlighted that most economic losses in high-wind hazard areas are due to the breach of the building envelope (e.g., Chen et al., 2016; Yang et al., 2018). This includes roof panel uplift, roof-to-wall connection failure, and roof system damage, among other failure modes. Once the roof is damaged or even partially/totally collapsed, walls may lose lateral support, heavily affecting the entire construction's global stability. CH and residential asset roofs in Southeast Asian countries are commonly made of wood/steel frame and lightweight metal sheets (LWMSs); this structural typology is the main focus of this study. Steel screws and nails are used as fasteners; considering the reduction of their structural capacity due to corrosion is also essential.

Several past studies have addressed the development/use of risk assessment methods and fragility derivation for structural and non-structural components of wood-frame roofs with LWMSs under extreme wind loads (e.g., Masoomi et al., 2018; Song et al., 2019; Vickery et al., 2006, among many others). Most of the existing studies explicitly model wind-induced demands and component capacities in a full probabilistic fashion, in a few cases also considering corrosion models for fasteners/roof-panel and climate-change impact on the wind risk assessment outputs (e.g., Pita et al., 2015; Qin and Stewart, 2019; Stewart et al., 2018). These existing studies often rely on refined numerical (structural) models requiring specific/detailed data about the analyzed asset (e.g., roof geometry, number/location of purlins, number/location of fasteners, material properties). The computational burden and data accuracy required to perform such analyses may prevent their use for wind risk prioritization for large building portfolios, particularly in developing countries. High population density, adaptive reuse of CH assets, and widespread material degradation are disruptive factors for data collection during field surveys (e.g., Sevieri et al., 2020). In this context, simplified scoring-based vulnerability/risk prioritization methods for building portfolios (e.g., Gentile et al., 2019; Pita et al., 2015) are often adopted. However, such methods are less appropriate for building-specific applications, and they do not enable structural capacity degradation and climate change impact to be adequately accounted for in the risk prioritization scheme.

The above gaps are addressed in this study by proposing a simplified simulation-based framework for typhoon risk assessment of CH-asset roofs. The proposed framework can be used for both risk prioritization at a building-portfolio level and a preliminary risk assessment at a building-specific level. Results from the analysis can be used to allocate resources/plan more detailed data-collection surveys for the definition of refined numerical models or to design strengthening interventions conceptually.

A simplified roof geometry is assumed in the proposed framework, requiring limited information about the structure under investigation and low computational costs. This enables the probabilistic modeling of wind-induced demands and component capacities as well as considering the effects of load redistributions due to fastener failure and fastener corrosion (for instance, due to the lack of maintenance activities). Variance-based sensitivity analysis (i.e., Sobol' indices; Sobol', 1993) based on polynomial chaos expansions of the limit state function is also performed within the proposed framework. Such a global sensitivity analysis allows one to investigate how the model outputs' uncertainty can be apportioned to different uncertainty sources in the model input (Saltelli et al., 2000). In the context of this study, sensitivity analysis is fundamental to understand which parameters affect more typhoon-risk variance, then deserving special attention (and more resources/investments) during data collection. In addition to a wind fragility model suitably defined for aging CH-asset roofs, this paper also investigates climate-change impact on typhoon risk assessment of CH-asset roofs at both portfolio and building-specific level. The use of new technologies (e.g., drones) for the collection of the input data required by the proposed framework is finally discussed with reference to a case study.

The analysis of 25 CH assets in Iloilo city, Philippines, demonstrates the feasibility of applying the proposed framework in practice. Three climate scenarios are considered to investigate how climate change may affect the wind risk profiles of the considered assets.

2. Typhoon risk assessment framework

In performance-based engineering, a given structure/structural component's performance is assessed through the probabilistic description of a set of decision variables (DVs) (e.g., Moehle and Deierlein, 2004; Cremen and Baker, 2018). Each DV is a quantitative proxy for the specific structural performance/damage in terms of metrics of interest to various stakeholders and/or society in general, e.g., direct repair cost, downtime, and affected people (casualties/injuries). In this study, direct economic losses (L) related to repair costs (of physical damage) are the considered DV, while the expected annual loss (EAL, i.e., integration of loss ratio over all possible annual frequencies of the considered hazard intensity) is the adopted risk metric (e.g., Grossi and Kunreuther, 2005),

$$\mathrm{EAL} = \sum_{v_i=0}^{v_{\max}} L\, Pr[L|DM] Pr[DM|IM = v_i]\; |\Delta\, \lambda_v(IM = v_i)|. \tag{1}$$

In the previous equation, IM is a wind intensity measure, probabilistically describing the hazard intensity at a site of interest; λ_v is the mean annual frequency of exceeding a given IM level v_i, and DM is a damage measure quantifying the structural damage due to wind load. In the context of typhoon risk assessment, the 3-sec gust speed (v, i.e., the highest 3-sec average wind speed within an observation period of 10 minutes) at 10 m height in open terrain (National Structural Code of the Philippines, NSCP, 2015) is used as an IM while the ratio (R_{damage}) between the number of damaged LWMSs and their total number is used as a DM. For practical reasons, a maximum IM level, capturing the upper bound of probabilistically significant events, is selected (i.e., $v_{\max}$ in Equation 1). Finally, $Pr[DM|IM = v_i]$ indicates the probability of DM conditional on the hazard intensity (usually referred to as fragility), while $Pr[L|DM]$ is the conditional probability of loss given the occurrence of damage. The calculation of $Pr[L|DM]$ requires the definition of a damage-to-loss (or consequence) model describing the (probabilistic) relationship between DM and DV (i.e., in terms of R_{damage} and economic losses in this context) (Vickery et al., 2006). Since no damage-to-loss models are specifically available for Filipino buildings, those developed by the Federal Emergency Management Agency (FEMA, 2014) in terms of direct repair costs for residential buildings in the USA are used in this study. This assumption is somehow justified by the fact that the prescriptions included in the Filipino building codes (NSCP, 2015) are entirely consistent with the recommendations of US building codes (see Sevieri et al., 2020 for a detailed analysis/mapping) across the years. Moreover, the damage-to-loss curves reported in Figure 1 are defined in terms of the percentage of building replacement value rather than in absolute terms. Hence, even if this specific aspect will require more investigation in future studies, it still allows one to illustrate the proposed framework and to obtain loss results for relative comparisons/risk prioritization exercises for the selected case-study portfolio.

The damage-to-loss curves adopted in this study consider direct repair costs associated with roof covering, roof framing, and content. It is worth noting that the damage-to-loss curves presented in this section represent the expected loss L given R_{damage}, that is $\mathbb{E}[L|R_{\mathrm{damage}}]$. This means that the consequence model's uncertainties are not considered in the risk assessment framework presented in this study. This is a limitation of this study as damage-to-loss uncertainties significantly affect the total loss distribution and its percentiles. However, according to Silva (2019), the mean loss ratio for a given IM level must not change regardless of the sources of uncertainty considered in the vulnerability modeling approach. When significant differences in this metric are noticed, the statistical model introduces a bias in the random variable. Therefore, when intensity-based losses or EAL are used as metrics in the definition of preliminary risk estimation at building specific level and/or risk prioritization at a portfolio level, as in the proposed method, the impact of such uncertainties is not expected to alter the result.

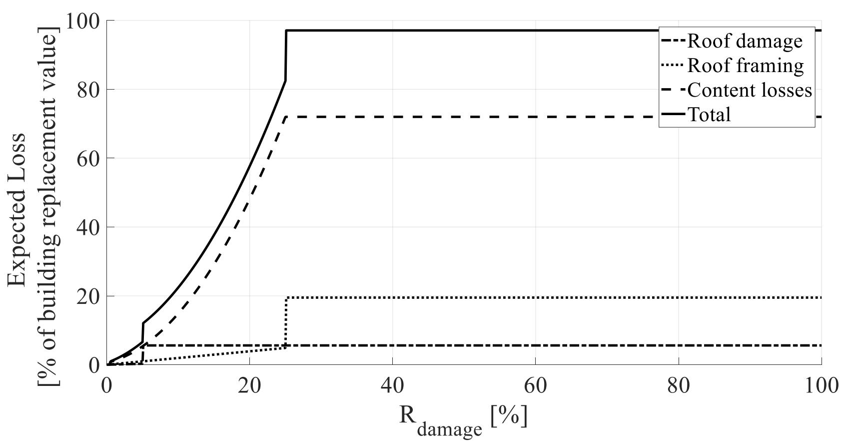

Figure 1. Damage-to-loss relationships adopted in this study.

The use of the same consequence model for all the assets relies on the assumption of a homogeneous building portfolio, at least from the exposure perspective. This means that all the assets within the analyzed portfolio should have similar construction features and similar replacement costs (so leading to coherent repair costs/direct loss estimates), contents, downtime, and intangible values. Focusing on this latter aspect, Sevieri et al. (2020) proposed an index-based multi-hazard risk prioritization method in which CH intangible value is considered by defining an ad-hoc cultural value index. The same approach could be easily applied in the proposed method, where the CH intangible value index could be used to weight the different risk prioritization indices purely based on EAL.

2.1 Wind hazard modeling and influence of climate change on the wind hazard profile

Quantifying climate-change impact on typhoon risk assessment outputs is among the specific objectives of this study. One of the main effects of climate change is the rise in the world's oceans' temperature. As their surface temperature increases, oceans provide more energy to convert into tropical cyclones (Elsner et al., 2008). According to Mei et al. (2015), this is the thermodynamic phenomenon due to climate change that will cause the globally averaged intensity of tropical cyclones to shift towards stronger storms, from being a category 3 (i.e., severe tropical storm) to a category 4 (i.e., typhoon) by the end of the 21^{st} century. Recent studies (e.g., Emanuel, 2011; Knutson et al., 2010) specifically discuss how the greenhouse warming will cause the globally averaged intensity of tropical cyclones to shift towards stronger storms, with intensity increases of 2-11% by 2100. Besides, climate change may also affect tropical storm frequencies, paths, and velocities. For instance, some recent extreme events in the Philippines (e.g., the 2011 tropical storm Washi, the 2012 typhoon Bopha, the 2013 typhoon Haiyan) have shown east-to-west trajectories rather than commonly observed southeast-to-northwest ones (Holden and Marshall, 2018). These variations of the environmental conditions may affect the wind hazard of the country and, ultimately, the wind risk profile of selected sites.

The Type I (Gumbel) distribution is generally adopted in the scientific literature (e.g., Garciano et al., 2005) and in structural codes (e.g., NSCP, 2015) to probabilistically model the 3-sec gust speed at 10 m height in open terrain (v). The climate change effect can be incorporated in the hazard model by modifying the cumulative distribution function (CDF) of the 3-sec gust speed ($\mathrm{F}_v(v, y)$) with a function ($\gamma_{\mathrm{mean}}(y)$) expressing the time-dependent percentage change in v (Stewart, 2016),

$$\mathrm{F}_v(v, y) = \exp\left(-\exp\left(-\left(\frac{\frac{v}{1+\frac{\gamma_{\mathrm{mean}}(y)}{100}} - v_g}{\sigma_g}\right)\right)\right). \quad (2)$$

In the previous equation, v_g and σ_g are the location and scale parameters of the CDF of v, respectively, while y (years) is the observation year. According to Garciano et al. (2005), in Iloilo City, where the case-study CH assets considered in this study are located (as discussed in the following sections), these parameters can be assumed as $v_g = 25.21\ \mathrm{m/s}$ and $\sigma_g = 5.75\ \mathrm{m/s}$. Several studies available in the scientific literature assume a time-dependent linear change in wind speed $\gamma_{\mathrm{mean}}(y)$ and discuss how different functional approximations do not really affect the typhoon risk assessment (e.g., Stewart, 2016; Stewart et al., 2018). In this study, three climate scenarios (CS) are assumed for the projected changes in wind speed over the next 50 years: CS_1 = 2%, CS_2 = 4%; and CS_3 = 8%. These climate scenarios are in agreement with the studies available in the scientific literature for similar geographic locations (e.g., Silang et al., 2014; Villarin et al., 2016). Considering various climate scenarios enables a proper investigation of climate-change impact on the typhoon risk assessment of the considered CH-asset roofs. Once new reliable climate projections will becomes available, they can be used to better calibrate time-dependent changes in the wind speeds for the Philippines or to directly update the Type I distribution parameters as for the case of other environmental loads (e.g., for snow load, Croce et al. 2018; Croce et al. 2019). Figure 2 shows the 3-sec gust speed values for different mean return periods (T_R) and the three considered climate scenarios. It is worth noting that the return period is directly related to $\mathrm{F}_v(v, y)$, that is $\mathrm{T}_R = 1/\left(1 - \mathrm{F}_v(v, y)\right)$.

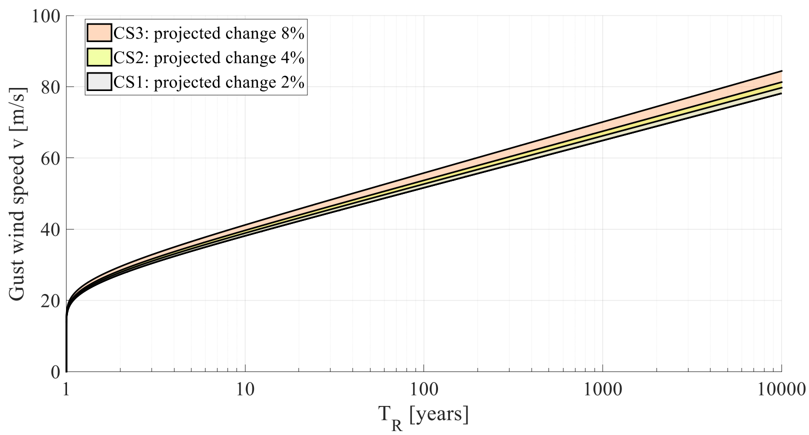

Figure 2. Gust wind speed versus mean return period for the three different climate scenarios (CSs).

3. Proposed fragility model

An LWMS is assumed to fail when a given number of associated fasteners (screws or nails) fails. The threshold defining the failure of an LWMS is treated as uncertain and described in detail below. Analyzing the roof failure down to the LWMS/fastener level facilitates incorporating fastener/roof-panel corrosion and load-redistribution across the roof (as fasteners progressively fail) into the fragility model. Therefore, the determination of the roof fragility (i.e., $Pr[DM|IM = v_i]$ in Equation 1) requires the calculation of the probability of failure (p_f) at LWMS/fasteners level, which is defined as

$$p_f = Pr[g(C, D) \leq 0], \tag{3}$$

where $g(C, D)$ is the limit state function, C is the uplift resistance (i.e., capacity) for pullout/pullover failure modes (i.e., the two failure mechanisms considered in this study and introduced in the following section), and D is the total load effect (i.e., demand). This latter includes two contributions: the uplift wind load W and the roof dead load Q, so that $D = W - Q$. In this way, Equation 3 can be rewritten as:

$$p_f = Pr[g(C, D) \leq 0] = Pr[C - D \leq 0] = Pr[C - (W - Q) \leq 0]. \tag{4}$$

In this study, the dead load Q is considered as deterministic, while both capacity C and wind uplift W are modeled probabilistically. This is a fundamental aspect to properly consider the uncertainties involved in defining both C and W.

The fragility model proposed in this study is based on a simplified geometry of the roof. Specifically, the analyzed CH roofs are divided into (N_{ms}) LWMSs, each of which is supported by a constant number of purlins (N_p) and connected through a constant number of fasteners (N_f). LWMSs are also assumed not interacting with each other, thus allowing the parallelization of the procedure and reducing the computational burden. Only a few information about the roof are thus needed to perform the fragility analysis, namely: N_{ms}, N_p, N_f, the distance between purlins (d_p), fastener typology/geometry, LWMS typology/geometry, and dead load (D); Figure 3.

When a fastener fails, its load is redistributed among the closest resisting elements until the equilibrium is achieved. This step requires the definition of a connectivity matrix for each LWMS. Once the safety of each LWMS is assessed, R_{damage} is calculated as the ratio of the number of failed LWMSs over N_{ms}. This procedure is repeated by varying the wind speed v needed for the definition of D.

Monte Carlo sampling is used to propagate the considered uncertainties. Once a wind speed v is selected, the uplift loads W are randomly generated for each fastener of each LWMS of the roof. For the same elements, pullout and pullover capacities are also randomly generated. A corrosion model is implemented to reduce the resisting sections of fasteners and LWMSs over time, thus reducing the capacity C. The starting degradation level is treated as a random variable to consider the heterogeneity of the conditions of different LWMS observed during field trips in developing countries (e.g., Sevieri et al., 2020). Figure 4 summarizes the main steps of the proposed fragility analysis.

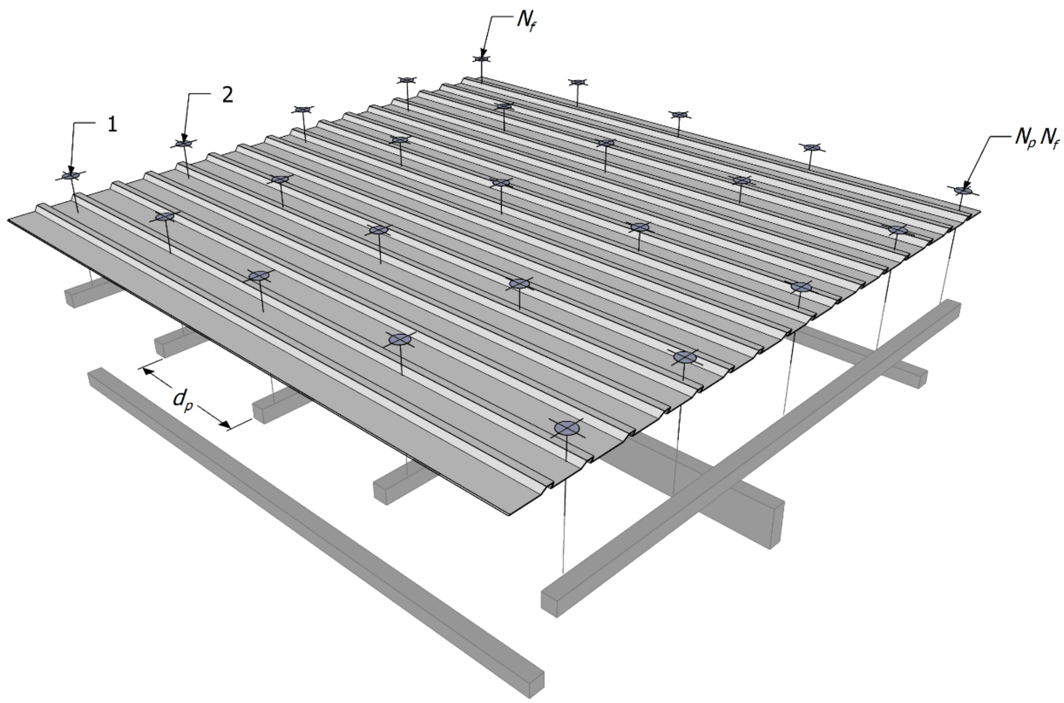

Figure 3. Reference metal sheet in the considered fragility model.

It is finally worth noting that fatigue-induced connection failure is not considered in the proposed study. A significant reduction of roof components' static uplift capacity due to highly fluctuating winds was reported in the literature, based on experimental testing (e.g., Mahendran and Mahaarachchi, 2002). To the authors' knowledge, no similar studies are available in the literature for CH roofs using LWMSs. More in general, the typhoon-risk prioritization of CH-asset roofs – as proposed in this study – should not be significantly affected if fatigue effects are neglected. In fact, most of the considered CH assets share similar roof-panel/purlin materials and fastener types. While neglecting fatigue effects may results in an underestimation of the absolute values of the fragility/risk estimates for the considered assets, considering fatigue effects would lead to a uniform reduction of the roof uplift capacity for all the considered assets, not affecting the relative 'ranking' and relative comparisons performed in the study.

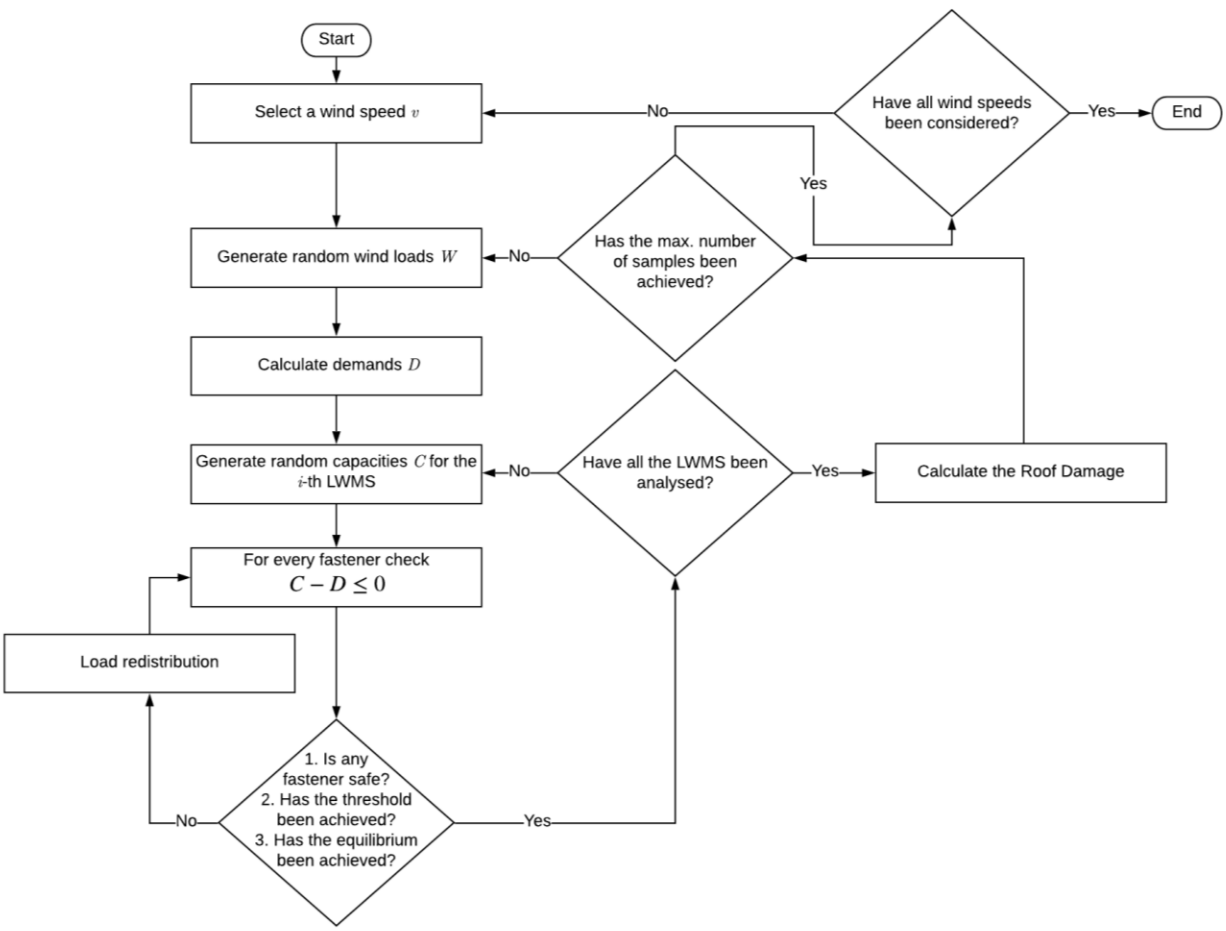

Figure 4. Flowchart of the proposed fragility model.

The following sub-sections are specifically tailored to Filipino CH assets, which are the focus of the case study considered in this paper. However, the proposed framework is general enough to be easily adapted to different roof typologies and then to different assets. This only requires the definition of specific input parameter distributions and, eventually, different capacity models, which might better describe other roof typologies.

3.1 Wind load

The NSCP 2015 provides wind load provisions entirely consistent with the American Society of Civil Engineers (ASCE) Standard 7-10 (ASCE, 2010) and based on findings of wind measurements and wind tunnel tests conducted over the past few years. Assuming that LWMSs, purlins, and fasteners can be considered as *components and claddings* (C&C), the uplift wind load W (N/m^2) is written as (ASCE, 2010; NSCP, 2015)

$$W = q_h\left(G_{\text{wind}}C_p - G_{\text{wind}}C_{pi}\right), \tag{5}$$

where q_h is the velocity pressure evaluated at the mean roof height of h; G_{wind} is the gust factor; C_p is the external pressure coefficient (NSCP 2015 Figures 207E.4-2A to 207E.4-7); and C_{pi} is the internal pressure coefficient (NSCP 2015 Table 207A.11-1). In both codes, q_h (N/m^2) is evaluated as:

$$q_h = 0.613\, K_h\, K_{zt}\, K_d\, v^2, \tag{6}$$

where K_h is an exposure factor accounting for the terrain exposure condition (NSCP 2015 Table 207E.3-1); K_{zt} is a topography factor; and K_d is a wind directionality factor accounting for the reduced probability of unfavorable building orientation and wind direction (NSCP 2015 Table 207A.6-1).

In this study, the parameter of Equations 5 and 6 are modeled as random variables, and their probability density functions (PDFs) are defined according to the scientific literature (Ellingwood and Tekie, 1999; Lee and Rosowsky, 2005) and reported in Table 1.

Table 1. Wind load statistics.

Parameters	Category	Mean	Coefficient of Variations (COV)	Statistical model	Reference
$G_{\mathrm{wind}}C_p$		see Table 2		Normal	
$G_{\mathrm{wind}}C_{pi}$	Partially enclosed	0.46	0.33	Normal	
K_h	Exposure B (0 – 9.1 m)	0.71	0.19	Normal	(Ellingwood and Tekie, 1999)
K_d		0.89	0.16	Normal	
K_{zt}		Deterministic (= 1)			

Given the orography of the territory of Iloilo City (i.e., the site of the case-study CH assets in this study), and the geometric features of the considered CH assets (i.e., two-story, plan-regular buildings), the exposure category B is selected for the definition of K_h. The topographic factor K_{zt} is assumed deterministic and equal to 1 for all the assets under investigation as they are located in a relatively small flat area close to the coastline. Moreover, the CH assets analyzed in this study are considered partially enclosed for the definition of $G_{\mathrm{wind}}C_{pi}$. According to the Filipino building code (NSCP, 2015), the category of enclosure of a specific building must be selected based on the opening area within the building facades. The CH assets in Iloilo City are usually characterized by open ground floors and large windows on the upper floors. However, they are located in a “crowded” urban context and are parts of building blocks. This reduces the number of surfaces exposed to wind. The gust pressure coefficient $G_{\mathrm{wind}}C_p$ varies depending on the LWMS location. LWMSs along the edge of the roof have higher external pressures than the interior ones. The statistics of $G_{\text{wind}}C_p$ are reported in Table 2, assuming a roof slope equal to 18°: this value is commonly adopted to facilitate the flow of rainwater. If different roof slopes are present in the analyzed portfolio, the statistics of the $G_{\text{wind}}C_p$ distributions can be adjusted through the value available in the scientific literature (Lee and Rosowsky, 2005).

Table 2. Statistics of the gust pressure coefficient $G_{\text{wind}}C_p$.

LWMS position		Mean	Coefficient of Variations (COV)	Reference
(Wind from all directions) 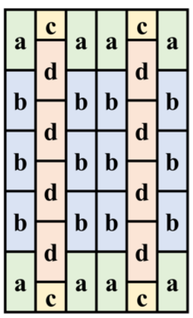	a	−1.768	0.12	
	b	−1.455	0.12	
	c	−1.425	0.12	(Lee and Rosowsky, 2005)
	d	−0.855	0.12	

It is finally worth noting that even though the proposed method considers a simplified roof geometry, and mainly that panels do not interact with each other, the roof slope and panel position still affect the result through the definition of the $G_{\text{wind}}C_p$ distributions.

3.2 Dead and total loads

The value of the dead load (Q) needed for the calculation of the total demand (D) depends on the weight of roof panel material and that of the roof system. This load counteracts the effect of wind uplift, thus stabilizing the roof and increasing its resistance. In this study, the dead load is modeled as deterministic and assumed to remain constant in time (i.e., added weight due to re-roofing, if any, is not considered here) and equal to 0.2 kN/m^2. This value can be easily found in the scientific literature for the same roof typology (e.g., Song et al., 2019; Stewart et al., 2018).

3.3 Uplift resistance

Two main failure mechanisms govern the uplift failure of a roof panel: (1) *pullout failure*, when a roof fastener (e.g., screw or nail) is pulled out from the holding member due to wind-induced uplift loading; and (2) *pullover failure*, when a roof panel fails/fractures while the connecting fastener is still intact within the holding members. Therefore, the capacity (C) of a roof panel mainly depends on the fastener typology (i.e., screws or nails) and the structural system's geometry (e.g., the distance between fasteners, the distance between purlins). Assuming that the forces due to the wind uplift act parallel to the length of the fasteners and perpendicular to the holding members, the nominal pullover resistance per screw and nail ($P_{n,over}$ in N) is defined, according to NSCP (2015), as

$$P_{n,over} = 1.5\ t\ d_w\ F_{u1}, \tag{7}$$

where, in the case of screws, t (mm) is the thickness of the member in contact with the screw head, d_w (mm) is the larger of the diameter of the washer and the screw head and F_{u1} (MPa) is the ultimate tensile strength of the member in contact with screw head or washer. In the case of nails, d_w is the diameter of the nail head.

The definition of the pullout resistance for screws $P_{n,out,screw}$ (N) is based on the design criteria provided by the NSCP (2015),

$$P_{n,out,screw} = 0.85\ t_c\ d\ F_{u2}, \tag{8}$$

where t_c (mm) is the lesser of the depth of penetration and thickness of the element not in contact with the screw head, d (mm) is the nominal screw diameter, and F_{u2} (MPa) is the ultimate tensile strength of the member not in contact with the screw head or washer.

When the roof structure is made of wood purlins, nails are generally used as fasteners. In this case, according to the US National Design Specification (NDS) for Wood Construction (AWC, 2017), the pullout capacity for a single smooth shank nail used as wood-to-wood and metal-to-wood connections $P_{out,nail}$ (N) can be expressed as

$$P_{out,nail} = K_w\, G_{\text{out}}^{5/2}\, d_s\, P, \tag{9}$$

where G_{out} is the specific gravity of the wood-based on oven-dry weight, d_s (mm) is the shank diameter of the nail, P (mm) is the penetration of the nail in the member holding the nail point, and K_w is a constant having a value of 9.515, which is converted from the original value of 1380 (in empirical unit) for SI unit consistency.

The parameters needed for the roof-panel capacity definition are treated as random variables to properly account for the epistemic uncertainties involved in the fragility calculation and 'balance' the proposed model's simplified geometry. In the case study presented in this paper, the geometric parameters of the resisting elements (i.e., d_w, t_c, d, d_s, P) are considered normally distributed with mean values equal to the nominal values measured during field surveys or assumed during the analysis. More specifically, 4d and 8d fasteners (i.e., nominal diameters equal to 2.9 and 3.3 mm, respectively) are usually found for such a roof typology (Dong and Li, 2016; Stewart et al., 2018). The coefficients of variations of these variables are derived from studies related to Filipino roofs available in the scientific literature (Alvarez et al., 2013; Song et al., 2019). Table 3 summarizes the statistical models for the parameters defining the pullout/pullover capacities adopted in this study. The nature of these uncertainties is epistemic. These variabilities are mostly related to measurement errors and the impossibility of adequately measuring each fastener. The statistics reported in Table 3 are referred to LWMSs with 0.79 mm thickness. F_{u2} and t_c refer to C-purlin of LC – 150×50×18×3 (NSCP, 2015), commonly adopted in this context as steel purlins.

Table 3. Capacity parameter statistics.

Parameters	Mean	Coefficient of Variations (COV)	Statistical model
t	0.79 mm	0.1	Normal
d_w	Nominal or assumed value	0.05	Normal
d	Nominal or assumed value	0.05	Normal
d_s	20% of d	0.025	Normal
P	Nominal or assumed value	0.25	Normal
F_{u1}	147 MPa	0.35	Log Normal
F_{u2}	215[a] MPa	0.10	Log Normal
t_c	Nominal or assumed value	0.025	Normal
G_{out}	Nominal or assumed value	0.25	Normal

It is worth noting that the reliability of the data collected on-site is often low, with several variables not recorded in the survey forms. When no specific data about the roof geometry and corresponding fasteners/roof panels are available, studies from the scientific literature (e.g. Alvarez et al. 2013, Dong and Li, 2016) can be used to define the probability distribution models, bias, and variability of the required capacity parameters. However, this still requires the knowledge of nominal values, which can be derived in different ways. For instance, roof inspections through new technologies (e.g., drones) would be the preferred option. However, when an extensive survey campaign cannot be afforded, nominal values can be calibrated based on those available for similar roof typologies, using engineering judgments. For instance, one can consider, for each missing value of a given variable, the (weighted) average of the recorded values for the same variable for other similar assets.

3.4 Corrosion effects

Corrosion can significantly reduce the effective section of fasteners and LWMSs, thus reducing roof panels' uplift resistance over time. This fundamental aspect is even more critical when the analyzed assets are located in developing countries and coastal regions. Lack of maintenance and airborne salinity further exacerbate corrosion effects.

The corrosion model adopted in this study is the one proposed by Nguyen et al. (2013). Two types of corrosions (Figure 5) are considered: embedded and atmospheric.

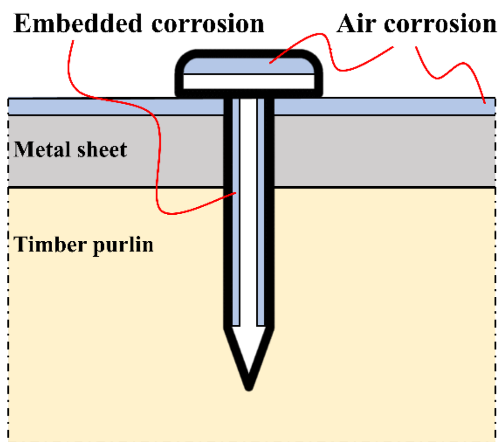

Figure 5. Corrosion model.

Atmospheric corrosion is due to corrosive agents within the surrounding air, such as airborne salinity and airborne pollution agents. The parts of the cladding exposed to the air, such as the heads of nails and screws as well as the LWMS surfaces, are affected by this type of corrosion. The air corrosion affects the pullout resistance by reducing t and d_w of equation 7.

The mean atmospheric corrosion depth, c_{atm} (μm), over a period of time y (years) is estimated by the following power-law equation,

$$c_{atm} = c_{0,atm}\, y^{n_{atm}}, \tag{10}$$

where n_{atm} is equal to 0.8 for steel fasteners and $c_{0,atm}$ (μm) is the atmospheric corrosion depth for the first year. According to Nguyen et al. (2013), $c_{0,atm}$ is a function of the time of wetness t_{wet} (%), the airborne salinity S_{air} (mg/m^2/day) and the airborne pollution of air P_{air} in terms of level of airborne sulfur dioxide (SO_2 μg/m^3):

$$c_{0,atm} = 0.5\, t_{wet}^{0.8}\, S_{air}^{0.5} + 0.1\, t_{wet}^{0.5}\, P_{air}. \tag{11}$$

The time of wetness is defined as the percentage of time in a year in which the relative humidity is above 80% and the temperature above 0°C. The average monthly relative humidity in the Philippines varies between 71% in March and 85% in September (Philippine Atmospheric Geophysical and Astronomical Services Administration, PAGASA, 2019); based on the average of all-weather stations in the Philippines, the mean annual temperature is 26.6°C. The coolest months fall in January with a mean temperature of 25.5°C, while the warmest month occurs in May with a mean temperature of 28.3°C (PAGASA, 2019). Based on an analysis of weather data from the PAGASA (2019), the factor t_{wet} for Iloilo City is estimated equal to 25%. This value is in agreement with those available in the scientific literature for countries with a similar weather (e.g., Dong and Li, 2016; Nguyen et al., 2013).

Airborne salt is generated primarily from the action of surf and ocean waves. No specific studies aimed at quantifying the airborne salinity S_{air} in the Philippines and, in particular, in Iloilo City are available. However, according to Slamova et al. (2012), the level of airborne salinity (expressed in terms of mg/m^2/day) in the Philippines is similar to the Vietnamese one, for which specific studies are available (Cole, 2000). Therefore, S_{air} in Iloilo City is assumed equal to 50 mg/m^2/day.

Finally, in this study, the content of sulfur dioxide for the calculation of P_{air} is assumed equal to 12 μg/m^3 (Department of environmental and natural resources, Government of the Philippines, 2015).

Corrosive agents, such as wood acidity and timber moisture content, contribute to the surrounding wood's embedded corrosion. Only parts inside the wood, such as the shank of nails, are affected. As in the case of atmospheric corrosion, the mean embedded corrosion depth (c_{emb}) (μm), over a period y is expressed by the following equation

$$c_{emb} = c_{0,emb}\, y^{n_{emb}} \quad , \tag{12}$$

where $c_{0,emb}$ (μm) is the embedded corrosion depth for the first year and the shape factor n_{emb} is equal to 0.6 for steel fasteners. For the case of untreated wood, commonly diffused in the Philippines, $c_{0,emb}$ is calculated with the following equation,

$$c_{0,emb} = f_{120}(BTM_{max}) + 0.3\, f_{120}(BTM_{mean}), \tag{13}$$

where f_{120} is the 120-day corrosion depth, and it is a function of the moisture content (M) (%) of the wood. The parameters BTM_{max} and BTM_{mean} are the seasonal maximum and annual mean value of the timber moisture content in service, respectively. According to Nguyen et al. (2013), f_{120} can be expressed as

$$f_{120}(M) = \begin{cases} 0 & if\ M \leq M_0 \\ 0.2\, C_{120}(M - M_0) & if\ M_0 < M < (M_0 + 5) \\ C_{120} & if\ M \geq (M_0 + 5) \end{cases} \quad , \tag{14}$$

where the parameters C_{120} and M_0 depend on the wood typology and acidity class.

Since a specific material testing campaign aimed at characterizing the wood of the analyzed CH-asset roofs has not been performed, the values of C_{120} and M_0 are derived from the scientific literature (Nguyen et al., 2013). Assuming that the analyzed roofs are made of hardwoods with acidity class 2 (pH=4-5), M_0 is equal to 15% and C_{120} is equal to 8 μm.

The mean (BTM_{mean}) and maximum (BTM_{max}) seasonal moisture contents can be calculated by applying the following equations:

$$BTM_{mean} = TM_{mean} + \Delta_{climate} + \Delta_{rain}; \tag{15}$$

$$BTM_{max} = BTM_{mean} + 0.1\, DF\, TM_{mean}, \tag{16}$$

where DF is the damping factor due to the lag in timber response, $\Delta_{climate}$ is the adjustment factor for the climate, Δ_{rain} is the rain factor, and TM_{mean} is the mean seasonal moisture content of a piece of wood. The adjustment factors for climate and rain account for factors affecting the climate of the area under investigation (e.g., distance to the coast) and the exposure to weather of a fastener, respectively. When the analyzed assets are located in coastal areas, as in the present case, these parameters can be assumed as $DF = 6.0$, $\Delta_{climate} = 2.5$ and $\Delta_{rain} = 17$ (Nguyen et al., 2013).

The mean seasonal moisture content of a piece of timber can be estimated by applying the following equation:

$$TM_{mean} = exp(1.9 + 0.05\, SEMC_{mean}), \tag{17}$$

where $SEMC_{mean}$ is the mean annual value of the surface equilibrium moisture content. Assuming an annual mean temperature equal to 28° and a mean annual humidity rate equal to 80% (PAGASA, 2019), $SEMC_{mean} = 16\%$ (United States Department of Agriculture, USDA, 2010).

Figure 6 shows the mean atmospheric and embedded corrosion depth, c_{atm} and c_{emb} respectively, adopted in this study.

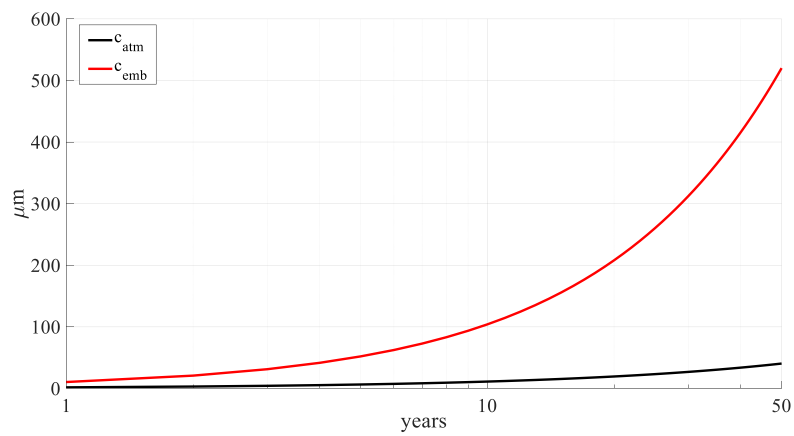

Figure 6. Atmospheric (c_{atm}) and embedded (c_{emb}) corrosion depths.

As previously mentioned, CH assets in developing countries show widespread and heterogenous corrosion, mainly due to the absence of periodic maintenance. Also, keeping track of the interventions on LWMSs and fasteners is practically impossible. Therefore, the initial embedded and atmospheric corrosion depths are uncertain and then herein treated as random variables. Specifically, due to the limited knowledge on the actual initial level of both embedded and atmospheric corrosions, a uniform probability distribution, ranging from 0 to 50 years, is herein adopted to model the age of all the fasteners and LWMSs belonging to the same cell. In this way, current corrosion values can be easily determined from Figure 6 (Equations 10 and 12). A changing climate would also affect the corrosion depth, both atmospheric and embedded, through temperature and humidity variation. However, in this study, only the climate change effect on the hazard profile of the area under investigation is considered. This choice is justified by the uncertainty related to estimating the initial corrosion conditions, as discussed above. A comprehensive understanding of how climate change affects corrosion depth would require an ad-hoc experimental campaign, but this is outside the current study's scope.

3.5 Fastener failure progression

Once a fastener fails, its load is redistributed among the adjacent resisting elements. This phenomenon is a crucial aspect that must be considered to properly model the failure progression of the corrugate metal sheets (Henderson et al., 2013). The redistribution rule adopted in this work is shown in Figure 7.

The 90% of the failed fastener's load is redistributed between those located on parallel purlins, while the remaining 10% goes to fasteners that are on the same purlin. Further details about the validation of this load redistribution model and its comparison with other models can be found in Konthesingha et al. (2015).

In the proposed procedure, the load is redistributed for each fastener failing until the equilibrium is achieved and the LWMS is still safe. Once the load is redistributed to other fasteners, they can fail, leading to rapid damage progression.

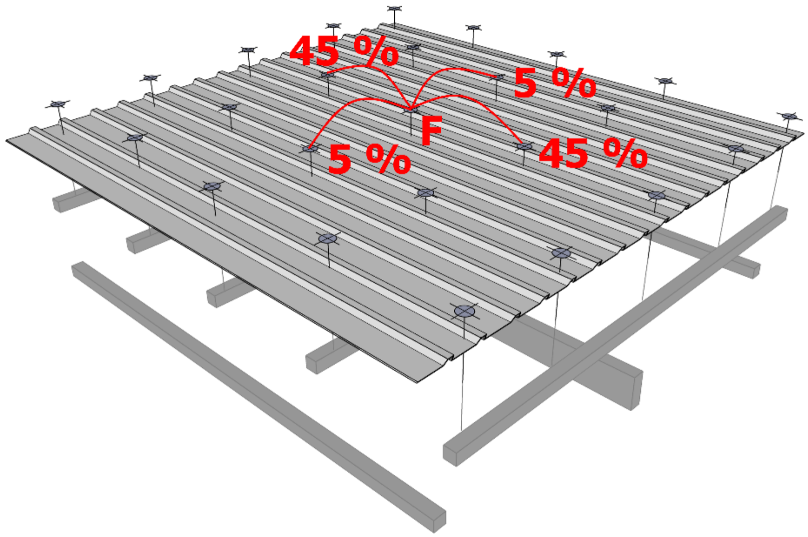

Figure 7. Load redistribution of failed fasteners.

3.6 Metal sheet failure criterion

The maximum number of failed fasteners (i.e., the threshold) to cause the failure of an LWMS is also treated as an uncertain parameter. This threshold varies depending on specific factors (e.g., wind direction, metal sheet dimension, location of the failed fasteners, wind pressure distribution) which can be considered only within high-fidelity numerical models. Although various thresholds related to specific cases have been proposed in the scientific literature (e.g., Henderson et al., 2013; Konthesingha et al., 2015), empirical evidence suggests that failure of a few fasteners generally results in metal sheet failure. Therefore, in this study, and according to Stewart et al. (2018), a triangular probability distribution bounded by 10% and 80% (the average is 33.3%) is adopted to define such threshold.

4. Typhoon risk prioritization approach

The proposed framework can be used for a preliminary/simplified typhoon risk assessment at a building-specific level, or for typhoon risk prioritization at a building-portfolio level, i.e., to assess the relative risk of various buildings within the considered portfolio. In this latter case, the same metric used to quantify typhoon risk can be adopted to define a prioritization index. Considering EAL as the risk metric of interest, the proposed typhoon risk prioritization index ($I_{TR,i,j,k}$) related to the k-th CH assets and considering the j-th observation year of the i-th climate scenario is defined as,

$$I_{TR,i,j,k} = \frac{(100-1)}{(\mathrm{EAL}_{\max,i,j}-\mathrm{EAL}_{\min,i,j})}\left(\mathrm{EAL}_{i,j,k} - \mathrm{EAL}_{\min,i,j}\right) + 1, \tag{18}$$

where $\mathrm{EAL}_{\max,i,j}$ and $\mathrm{EAL}_{\min,i,j}$ are the maximum and minimum EAL values within the analyzed portfolio, while $\mathrm{EAL}_{i,j,k}$ is the i,j,k-th expected annual loss.

5. Sensitivity analysis

The variance-based sensitivity analysis (Sobol', 1993) is used in this study to evaluate the impact of the considered uncertain parameters on the proposed fragility model. This method does not assume any type of linearity or monotonicity in the model and it is defined in a probabilistic framework. The Sobol' method decomposes the variance of the model output into fractions attributed to inputs or sets of inputs. Therefore, the i-th Sobol' index (S_i), related to the i-th input random variable, is defined as the ratio between the i-th partial variance ($\mathrm{VAR}_{\mathrm{parz},i}$) and the total variance of the output ($\mathrm{VAR}_{\mathrm{total}}$), that is $S_i = \mathrm{VAR}_{\mathrm{partial},i}/\mathrm{VAR}_{\mathrm{total}}$. Therefore, S_i expresses how the i-th parameter contributes to the total variance of the output.

The full description of the Sobol' indices require the evaluation of 2^n Monte Carlo integrals, where n is the number of random variables in the probabilistic problem. Its computation is not practically feasible unless the probabilistic problem's dimension and the computational burden of the model are sustainable. Therefore, first and second-order approximations of the Sobol' indices are generally computed (Sudret, 2008).

Alternatively, the Sobol' indices can be calculated by exploiting the Sobol' decomposition of the polynomial chaos expansion (PCE) of the uncertain model response (Xiu, 2010). In fact, according to Sudret (2008), once a PCE approximation of the model output is available, the Sobol' indices can be easily derived analytically with no additional cost. Only simple mathematical operations are needed to compute Sobol' indices from the expansion coefficients. On the other hand, this requires constructing a reliable PCE of the model (i.e., PCE characterized by low approximation error); for further details on these aspects, the reader may refer to Sevieri et al. (2019). The PCE belongs to the family of spectral methods for the propagation of uncertainties through deterministic models. In the context of stochastic modeling, this approach relies on orthogonal basis functions to construct a so-called response surface of the uncertain model output. The resulting response surface allows straightforwardly solving the forward problem (i.e., derivation of the main statistics of the uncertain model output) as well as surrogating the model output in optimization or reliability problems, thus reducing the computational burden. For instance, Sevieri and De Falco (2020) applied this technique for the definition of physics-based predictive models (i.e., physics-based machine learning) for the static and dynamic real-time control of strategic infrastructures.

Since the fragility model proposed in this study is sufficiently smooth, a reliable PCE of $g(C, D)$ can be easily computed. The Sobol' indices are thus calculated by following the PCE approach. For the sake of simplicity, it is possible to assume that all the random parameters that describe C and D are collected in a vector $\boldsymbol{\theta}$, while the deterministic ones are collected in $\mathbf{x}$, that is $g(\mathbf{x}, \boldsymbol{\theta})$. The PCE $\hat{g}(\mathbf{x}, \boldsymbol{\theta})$ of the limit state function can be written as,

$$g(\mathbf{x},\boldsymbol{\theta}) \approx \hat{g}(\mathbf{x},\boldsymbol{\theta}) = \sum_{\alpha\in\mathbf{I}} \mathbf{u}^{(\alpha)}(\mathbf{x})\ \boldsymbol{\Psi}_\alpha(\boldsymbol{\theta}), \tag{19}$$

where $\mathbf{u}^{(\alpha)}$ is the matrix of the combination coefficients of the orthogonal basis functions collected in $\boldsymbol{\Psi}_\alpha(\boldsymbol{\theta})$ and $\mathbf{I}$ the finite multi-index set. The orthogonality condition of the basis functions $\boldsymbol{\Psi}_\alpha(\boldsymbol{\theta})$ enables approximating the variance of $g(\mathbf{x},\boldsymbol{\theta})$ ($\mathrm{VAR_{total}}$) as:

$$\mathrm{VAR_{total}} = \mathrm{Var}[g(\mathbf{x},\boldsymbol{\theta})] \approx \widehat{\mathrm{VAR}}_{\mathrm{total}} = \mathrm{Var}[\hat{g}(\mathbf{x},\boldsymbol{\theta})] = \sum_{\alpha\in\mathbf{I}} \mathbf{u}^{(\alpha)}(\mathbf{x})\ \left(\boldsymbol{\Psi}_\alpha(\boldsymbol{\theta})\right)^2. \tag{20}$$

Defining the finite multi-index $\mathbf{J}$ (that is a subset of $\mathbf{I}$), such that only the indices related to the i-th random variables (i.e., input parameter) are nonzero, the i-th partial variance is then

$$\mathrm{VAR}_{\mathrm{partial},i} \approx \widehat{\mathrm{VAR}}_{\mathrm{partial},i} = \sum_{\beta\in\mathbf{J}} \mathbf{u}^{(\beta)}(\mathbf{x})\ \left(\boldsymbol{\Psi}_\beta(\boldsymbol{\theta})\right)^2. \tag{21}$$

The i-th PCE-based Sobol' index ($\hat{S}_i$) can be thus defined as:

$$\hat{S}_i = \frac{\widehat{\mathrm{VAR}}_{\mathrm{partial},i}}{\widehat{\mathrm{VAR}}_{\mathrm{total}}}$$

(22)

Sobol' indices derived through the PCE of $g(\mathbf{x},\boldsymbol{\theta})$ also provide information about the impact of uncertain model parameters on the probability of failure (Equation 4), and ultimately on the calculation of fragility, vulnerability, and loss curves.

Having only normally and log-normally distributed random variables in the case study (Tables 1 and 3), 4$^{\mathrm{th}}$ order Hermitian polynomials are used to define the PCE. The Bayesian procedure proposed by Rosić and Matthies (2017) is finally used to calculate the combination coefficients $\mathbf{u}^{(\alpha)}$.

It is worth noting that the PCE can be applied for both implicit and explicit problems. In fact, as for any other sampling-based uncertainty quantification method, only analysis results related to randomly generated input sets are required. At this stage, the main difference between the PCE and sampling-based approaches is that model solutions are used to calibrate the coefficients of the PCE basis. Finally, because of the orthogonality conditions of the basis functions, output statistics can be easily determined through algebraic computations.

6. Case study

6.1 Filipino cultural heritage assets

Recent catastrophic events, such as the 2013 super Typhoon Yolanda (international codename: Haiyan), have emphasized Filipino structures' vulnerability against extreme winds. This scenario is likely to be worsened in the future because of the impact of climate change on typhoon frequencies and resulting wind speeds, as discussed above. Indeed, the 2019 Pacific typhoon season was the costliest ever recorded. It was an above-average year with a grand total of 29 named storms, 17 typhoons, and four super typhoons. In 2019 the Philippine Area of Responsibility (PAR) experienced 17 typhoons, the costliest of which was the year's penultimate Pacific tropical cyclone, Typhoon Kammuri, which was known locally as Tisoy.

Relatively recent reinforced concrete (RC) frame-type structures and unreinforced masonry (URM) buildings with limited architectural and/or cultural features are often part of the Filipino CH portfolio. Differently from the criteria applied by the United Nations Educational, Scientific and Cultural Organization (Vecco, 2010) for the definition of CH assets, the Filipino law does not explicitly consider subjective features of the buildings such as the architectonical value and socio-cultural factors. The only 'objective' feature, which defines a building as a CH asset is the year of construction (Filipino Republic Act no. 10066, 2009). Structures that are at least fifty years old can be declared to be a "Heritage House" by the National Historical Commission of the Philippines (NHCP).

Twenty-five Filipino CH assets (Figure 8) were surveyed during a field trip in Iloilo City, Philippines, in July 2019 by a research group composed of members from the University College London (UCL, United Kingdom), the De La Salle University (DLSU, Philippines) and Central Philippines University (CPU, Philippines), as part of the *Cultural Heritage Resilience & Sustainability to multiple Hazards* (CHeRiSH) project (Sevieri et al., 2020). Iloilo City is a key heritage hub for tourism in the Philippines. It is one of the most highly urbanized cities of the south-eastern tip of Panay island in the Philippines (Philippine Statistics Authority, 2016) and the province's capital city. Fine examples of historic RC and URM buildings built in the first half of the 20th century, during the American colonization, can be found in the historic street Calle Real (Iloilo City Cultural Heritage Conservation Council, ICCHCC, 2010). Most of them are two-story, plan-regular buildings; in addition to wood/steel-frame roofs with LWMSs (19 CH assets in total), concrete flat roofs (6 CH assets) can also be found.

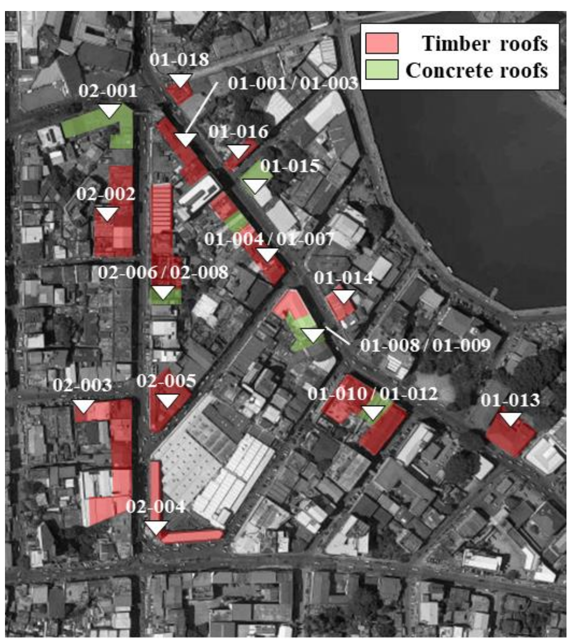

Figure 8. Surveyed CH buildings in Iloilo city, Philippines.

New technologies for data collections, such as photogrammetry, drones, thermal and omnidirectional cameras, facilitated the data-collection process during the fieldwork. Drones have been extensively used for façade and roof inspections. Figure 9 shows two inaccessible roofs; the drone was the only practicable tool for collecting roof data/information. The only limitation on drones' use was the strong wind during the fieldwork, which affected the flight capability.

Figure 9. Two samples of Filipino CH-asset roofs.

Particularly important is the entity of the corrosion affecting both LWMSs and fasteners. Figure 9 shows widespread heterogeneous corrosion, which is clearly due to a lack of maintenance activities.

6.2 Sensitivity analysis of fastener limit states

The Sobol' indices of $g(C, D)$ are calculated for both pullout and pullover failure mechanisms (Equations 7, 8, and 9) by varying the gust wind speed v from 0 to 100 m/s (Figure 10). For small gust wind speeds (black lines in Figure 10), the Sobol' indices show that the variability of the capacity-related variables affects the variation of the results more than the demand-related variables. In the case of roof-panel pullover and screw pullout (Figures 10a and 10b), the variation of the strength parameters F_{u1} and F_{u2} leads to the highest Sobol' indices (around 0.9 in both cases). In the case of nail pullout (Figure 10c), the variability of the specific gravity of the wood G_{out} is the factor that affects most the variation of the result. These results are justified by the fact that F_{u1}, F_{u2} and G_{out} are the parameters with the highest variability (Table 3). In addition, G_{out} is raised to $5/2$ in Equation 9, so the impact of its variation is even higher.

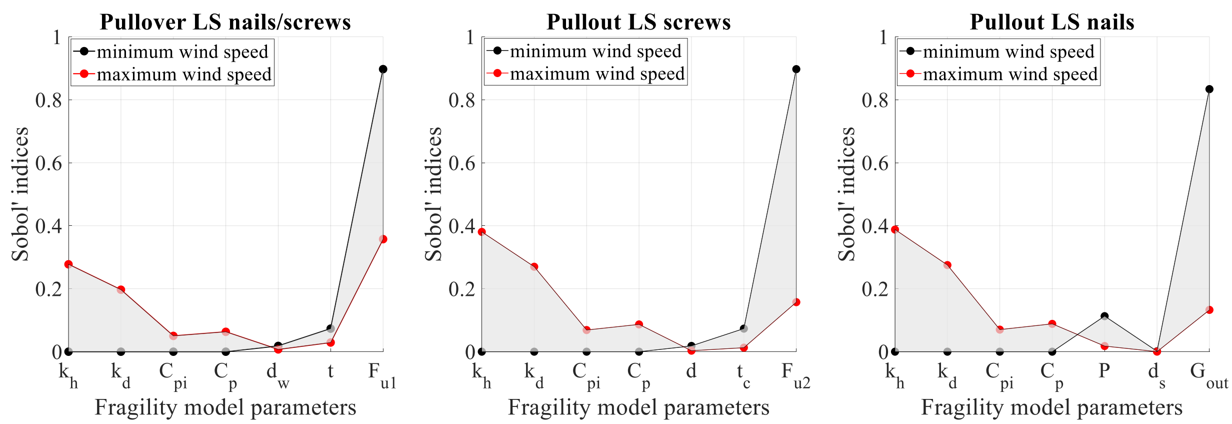

a) b) c)

Figure 10. Sobol' indices: a) Pullover LS of nails/screws, b) Pullout LS of screws and c) Pullout LS of nails. For the sake of clarity G_{wind} has been omitted in the Figure.

For high values of the gust wind speed, the variation of the random parameters used for the wind uplift definition affects the output variability more than the capacity parameters. For all the failure mechanisms, the exposure factor K_h is the most affecting parameter. This is mainly due to the its variability which is higher than the variability of the other demand parameters except that for $G_{\text{wind}}C_{pi}$. However, $G_{\text{wind}}C_{pi}$ is subtracted to $G_{\text{wind}}C_p$ (Equation 5) that has higher absolute values and smaller variance. Therefore, the effect of the variation of $G_{\text{wind}}C_{pi}$ is strongly mitigated.

As mentioned in Section 4, these findings also hold when looking at the value of the probability of failure. In this latter case, Sobol' indices may have different absolute values, compared to the $g(C, D)$ case, but same relative impact. These results suggest that a sensible reduction of the epistemic uncertainty effects on the upper tail of fragility curves can be achieved by improving the characterization of the structural demand D.

6.3 Fragility analysis

The fragility analysis has been carried out for all the 19 CH assets previously described by varying the gust wind speed v from 0 to 100 m/s with 2 m/s steps and by increasing the corrosion depths through the variation of y (Equations 10 and 12) by considering 10-year steps from 0 to 50 years. One million samples are considered within the Monte Carlo analysis to calculate the probability of failure (p_f, Equation 3) for a given IM with an approximation error (of the mean) of the order of 10^{-3}. A lognormal CDF is used to fit the analysis results by applying the maximum likelihood estimation (MLE) method (Baker, 2015).

For the sake of brevity, only the fragility curves for buildings with ID '01-001' and '02-003' (Figure 8) are described in this section. It is worth noting that the fragility curves derived for the other CH assets under investigation are in good agreement with the results presented in this section. The building '01-001' has 2.6-mm shank diameter screws with a 500-mm spacing. Whereas, the building '02-003' has 2-mm shank diameter nails with 250-mm spacing. When fragility curves are calculated for $y = 0$, so without increasing the initial corrosion depths, the two CH-asset roofs show similar fragility relationships (Figure 11). When y is increased, the corrosion affects more the roof '02-003' (Figure 11b) than the roof '01-001' (Figure 11a); in fact, the distance among fragility curves is more considerable in Figure 11b. This is mainly due to the fact that nails are affected by both embedded and atmospheric corrosion (Section 2.3.4), because of the use of wood purlins.

In contrast, screws are generally subjected to only atmospheric corrosion, which is generally smaller than the embedded one (Figure 6). Corrosion's influence also depends on the geometry of the roof structural system (e.g., fastener spacing, the distance between purlins) and the diameter of the fasteners. In general, the fragility curves derived in this study show that CH-asset roofs with nails as fasteners are more sensitive to corrosion than the screw ones.

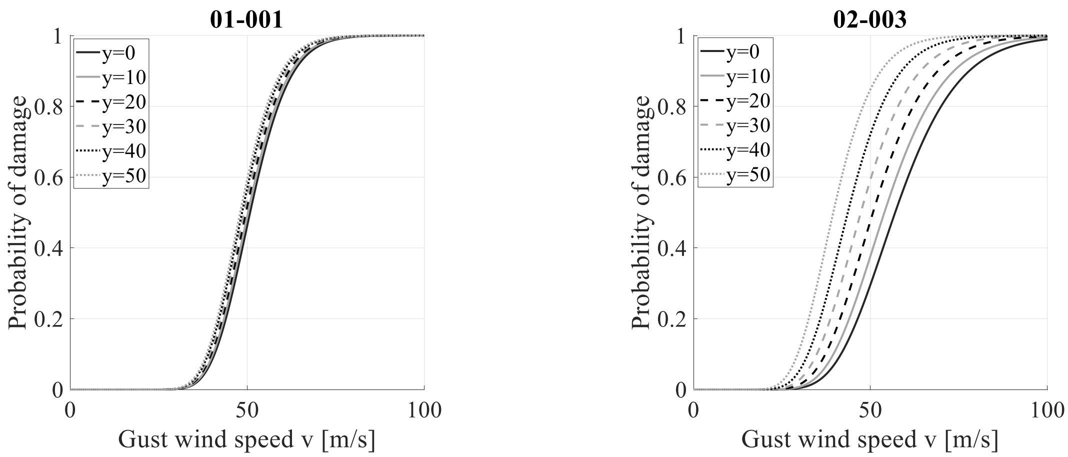

a) b)

Figure 11. Fragility curves derived for different observation years (y): a) building 01-001 (screws), b) building 02-003 (nails).

The results discussed in this section are in line with those available in the scientific literature for similar roof typologies (e.g., Stewart et al., 2018, Song et al., 2020), thus somehow validating the proposed fragility model. One should note that a validation of the whole procedure in terms of observed losses is unfeasible because of the lack of public data, such as insurance claims. Even when post-event loss data are available, they are usually characterized by high aggregation levels (e.g., for significantly larger geographic areas and building portfolios) rather than for specific, smaller building portfolios (as the one considered in this study).

6.4 Risk assessment

Loss curves (Figure 12) calculated considering the observation year equal to 0 are very close, thus reflecting the fragility curves' result. The variation of the observation year affects more the roof '02-003' (nails) than the '01-001' one (screws). This is mainly due to the effect of corrosion effect rather than climate change, as explained before. It is worth noting that the loss curves presented in this section are derived considering the expected values of damage-to-loss curves $\mathbb{E}[L|R_{\text{damage}}]$ (section 2). A comprehensive discussion of this problem would require considering the uncertainty related to the damage-to-loss curves, which means to consider $p[L|R_{\text{damage}}]$.

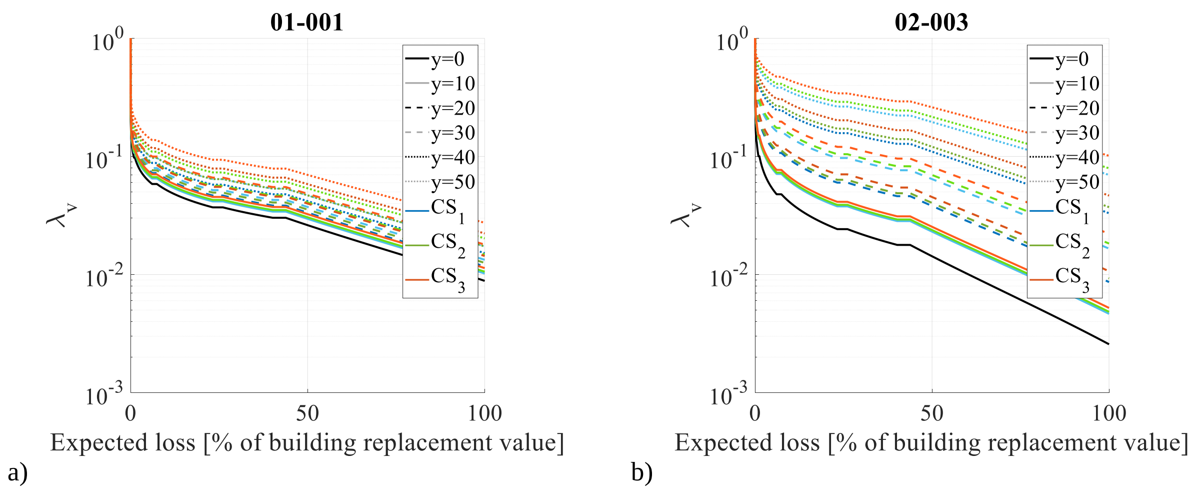

Figure 12. Loss curves derived for different observation years (y) and for different climate scenario (CS): a) building 01-001 (screws), b) building 02-003 (nails).

The loss curves are finally used to calculate the EAL for each CH assets considering different CS and observation years. A discount factor r equal to 4% is considered to refer EAL calculated for different observation years considering different CS to the same year. This can be easily done by dividing each EAL by $(1 + r)^y$.

The EAL in terms of percentage of building replacement value for all the 19 CH assets is reported in Table 4 for the three different climate scenarios.

CH-asset roofs with nails as fasteners show higher annual risks compared to those with screws. Again, this is mainly due to how corrosion affects screws and nails in different ways. However, as for fragility, vulnerability, and loss curves, other parameters, such as spacing between fasteners and purlins, significantly affect the risk assessment.

Table 4. EAL in terms of % of building replacement value.

CH ID	y = 0 [%]	y = 20 [%]	y = 50 [%]	CH ID	y = 0 [%]	y = 20 [%]	y = 50 [%]
01-001	3.2	CS1: 7.5 CS2: 7.7 CS3: 8.1	CS1: 9.7 CS2: 11.4 CS3: 12.6	01-014	20.8	CS1: 42.9 CS2: 44.1 CS3: 46.3	CS1: 70.1 CS2: 75.8 CS3: 79.5
01-002	5.4	CS1: 12.4 CS2: 12.6 CS3: 13.2	CS1: 17.4 CS2: 18.2 CS3: 20.0	01-016	11.5	CS1: 28.7 CS2: 29.3 CS3: 30.5	CS1: 44.9 CS2: 46.8 CS3: 50.7
01-003	1.9	CS1: 4.4 CS2: 4.5 CS3: 4.7	CS1: 6.3 CS2: 6.6 CS3: 7.4	01-018	2.1	CS1: 4.9 CS2: 5.0 CS3: 5.4	CS1: 7.0 CS2: 7.5 CS3: 8.3
01-004	7.5	CS1: 17.2 CS2: 17.6 CS3: 18.4	CS1: 24.3 CS2: 25.4 CS3: 27.7	02-002	1.6	CS1: 3.8 CS2: 3.9 CS3: 4.0	CS1: 5.5 CS2: 5.8 CS3: 6.5
01-006	4.9	CS1: 13.3 CS2: 13.6 CS3: 14.3	CS1: 23.4 CS2: 24.6 CS3: 27.2	02-003	2.4	CS1: 6.1 CS2: 6.4 CS3: 6.7	CS1: 14.6 CS2: 15.9 CS3: 18.0
01-007	3.4	CS1: 9.2 CS2: 9.5 CS3: 10.0	CS1: 16.6 CS2: 17.6 CS3: 19.6	02-004	CS1: 16.4 CS2: CS3:	CS1: 37.3 CS2: 38.0 CS3: 39.3	CS1: 51.82 CS2: 53.7 CS3: 57.7
01-008	0.3	CS1: 0.7 CS2: 0.7 CS3: 0.8	CS1: 1.1 CS2: 1.1 CS3: 1.3	02-005	CS1: 2.0	CS1: 6.2 CS2: 6.5 CS3: 6.9	CS1: 14.4 CS2: 15.7 CS3: 17.7
01-010	37.3	CS1: 71.6 CS2: 72.9 CS3: 73.8	CS1: 87.1 CS2: 88.5 CS3: 89.4	02-007	0.0	CS1: 0.0 CS2: 0.0 CS3: 0.1	CS1: 0.1 CS2: 0.1 CS3: 0.1
01-012	0.11	CS1: 0.3 CS2: 0.3 CS3: 0.3	CS1: 0.42 CS2: 0.42 CS3: 0.5	02-008	3.7	CS1: 9.3 CS2: 9.5 CS3: 10.0	CS1: 14.8 CS2: 15.6 CS3: 17.4
01-013	0.96	CS1: 2.3 CS2: 2.3 CS3: 2.5	CS1: 3.3 CS2: 3.5 CS3: 3.9				

The results reported in Table 4 confirm the previous findings, i.e., corrosion may affect the results of the risk assessment exercise more than climate change. In fact, the comparison between the EAL for different CSs, assuming the same y value, shows a little variation of the results. This seems to highlight that climate change has little impact on the typhoon risk assessment. Whereas, the comparison between EAL related to the same CS but for different y values shows higher variability of the result. In view of the conclusion derived in the previous section for the fragility curves (i.e., fragility curves are strongly affected by corrosion), the variation of the EAL (Table 4) seems to be mainly due to the material degradation (i.e., corrosion in this study).

It is worth noting that a parallelized Matlab® code has been developed to implement the proposed method. The computer used for the analysis of the case study (19 roofs composed of 3583 fasteners in total) has an Intel® core™ i7-8750H CPU @ 2.20 GHz with 16 Gb RAM, and it required 290 seconds to be completed (including the derivation of Sobol' indices).

6.5 Typhoon risk prioritization

The proposed typhoon risk prioritization index ($I_{TR,i,j,k}$) (Section 3) is finally calculated for the three considered CS by exploiting the results derived in the previous section. The resulting indices (Figure 13) are arbitrarily categorized into three groups, respectively "green", "yellow," and "red" tags by defining two thresholds. As a proof of concept, in this study, the thresholds are selected to be equal to 33% and 66% for the calculated typhoon risk index. The results reported in Figure 13 show that the variation of the reference year of analysis leads to a small variation of the prioritization index. This fact indicates that even if corrosion and climate change affect the risk analysis at a building-specific scale (previous section), the initial conditions of the analyzed CH assets are more important for the definition of the typhoon risk prioritization scheme.

Finally, the influence of climate projections can be assessed by comparing the prioritization schemes derived for the three different climate scenarios. Only small variations of the prioritization indices can be observed in Figure 13 due to the considered climate scenario. These results reveal that climate change affects more the risk analysis at a building-specific scale than the risk prioritization at a building-portfolio level.

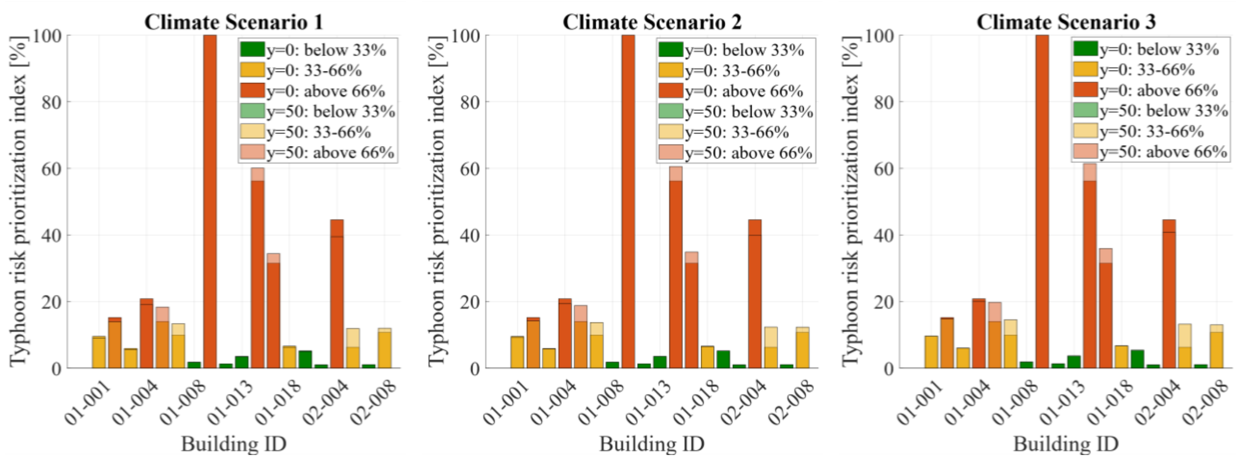

a) b) c)

Figure 13. Typhoon risk prioritization index: a) climate scenario 1, climate scenario 2 and c) climate scenario 3.

7. Conclusions

This paper introduced a simulation-based framework for CH-asset roof fragility derivation and risk assessment in which roof panel pullout and pullover failure mechanisms, corrosion effects, and load redistribution (after fastener failure) have been explicitly modeled. The considered CH-asset roofs are made of wood/steel frames and lightweight metal sheet (LWMSs) with steel screws and nails used as fasteners. A simplified model for the roof geometry, at the base of the proposed approach, has enabled one 1) to reduce the required computational burden for fragility assessment; and 2) to probabilistically model capacities/demands. The proper balance between refinement level and uncertainty propagation makes the proposed approach especially suitable for both risk prioritization at a building-portfolio level and preliminary risk assessment at a building-specific level. Finally, the impact of climate-change scenarios on the typhoon risk assessment results has been investigated by modifying the wind hazard profile for the site under investigation.

The analysis of 25 CH assets in Iloilo City, Philippines, has shown the feasibility of the proposed approach in practice and has enabled the evaluation of the impact of climate-change scenarios on both risk assessment at a building-specific level and on the proposed risk prioritization scheme. The results of the analysis have revealed that corrosion may strongly affect the fragility results for the considered CH-asset roofs. Therefore, given the lack of maintenance activities in several developed countries around the world, corrosion effects must be explicitly considered in the typhoon fragility/risk assessment. Results of the analysis have also shown that considered climate-change scenarios affect more the risk assessment estimates at building specific level than the prioritization scheme.

This study included a detailed uncertainty characterization for all the random variables involved in the proposed framework (e.g., those related to both wind-induced demands and component capacities as well as climate-change and corrosion scenarios). The uncertainty associated with the damage-to-loss model was instead neglected. While this uncertainty can significantly affect the total loss distribution, it does not significantly alter the assessment results in terms of expected annual losses, as proposed in this study.

It is worth highlighting that fatigue-induced connection failure was not considered in the proposed analysis. A significant reduction of roof components' static uplift capacity due to highly fluctuating winds is reported in the literature, based on experimental testing. The typhoon-risk prioritization of CH-asset roofs – as proposed in this study – should not be significantly affected if fatigue effects are neglected. In fact, most of the considered CH assets share similar roof-panel/purlin materials and fastener types. While neglecting fatigue effects may results in an underestimation of the absolute values of the fragility/risk estimates for the considered assets, considering fatigue effects would lead to a uniform reduction of the roof uplift capacity for all the considered assets, not affecting the relative ‘ranking’ and relative comparisons performed in the study.

Acknowledgments

This study was performed in the framework of the “CHeRiSH: Cultural Heritage Resilience & Sustainability to multiple Hazards” project funded by the UK British Council. The University of the Philippines Visayas (UPV), the Central Philippine University (CPU), and the De La Salle University (DLSU), Manila, are acknowledged for the technical support during the fieldwork.

References

Alexander, D.E., 2013. Resilience and disaster risk reduction: An etymological journey. Nat. Hazards Earth Syst. Sci. 13, 2702--2716. https://doi.org/10.5194/nhess-13-2707-2013

Alvarez, I.P.R., Colobong, J.A.M., Decal, C.Q., Tan, A.B.S., 2013. Pull-Out and Pull-Over Failure Probability of Residential House Roofs due to Extreme Wind Speeds: a Case Study in Malate, Metro Manila. BSc thesis, De La Salle University.

American Society of Civil Elilgineers (ASCE), 2010. ASCE 7-10, American Society of Civil Engineers, Minimum Design Loads for Buildings and Other Structures (ASCE/SEI 7-10). American Society of Civil Engineers, Reston, VA, USA.

American Wood Council (AWC), 2017. National Design Specification for Wood Construction. Leesburg, VA.

Association of structural engineers of the Philippines, 2015. National Structural Code of the Philippines. Manila.

Baker, J.W., 2015. Efficient analytical fragility function fitting using dynamic structural analysis. Earthq. Spectra. 31 (1), 579-599.

Chen, S.E., Leeman, M.E., English, B.J., Kennedy, A.B., Masters, F.J., Pinelli, J.P., Pang, W., Rullan-Rodriguez, J.A., Satyanarayana, P., Calvo, J., Murugan, B., Natarajan, C., 2016. Basic

Structure System Rating of Post-Super Typhoon Haiyan Structures in Tacloban and East Guiuan, Philippines. J. Perform. Constr. Facil. 30 (5).

Cole, I.S., 2000. Mechanism of atmospheric corrosion in tropical environments, in: Marine Corrosion in Tropical Environments. American Society for Testing and Materials, pp. 33–47.

Cremen, G., Baker, J.W., 2018. Quantifying the benefits of building instruments to FEMA P-58 rapid postearthquake damage and loss predictions. Eng. Struct. 176, 243–253.

Croce, P., Formichi, P., Landi, F., 2019. Climate Change: Impacts on Climatic Actions and Structural Reliability. Appl. Sci. 9 (24), 5416.

Croce, P., Formichi, P., Landi, F., Marsili, F., 2018. Climate change: Impact on snow loads on structures. Cold Reg. Sci. Technol. 150, 35–50. https://doi.org/10.1016/j.coldregions.2017.10.009

Department of environmental and natural resources, Government of the Philippines, 2015. National air quality status report (2008-2015).

Dong, Y., Li, Y., 2016. Reliability of Roof Panels in Coastal Areas Considering Effects of Climate Change and Embedded Corrosion of Metal Fasteners. ASCE-ASME J. Risk Uncertain. Eng. Syst. Part A Civ. Eng., 2 (1). https://doi.org/10.1061/AJRUA6.0000851

Ellingwood, B.R., Tekie, P.B., 1999. Wind load statistics for probability-based structural design. J. Struct. Eng. 125, 453–463. https://doi.org/10.1061/(ASCE)0733-9445(1999)125:4(453)

Elsner, J.B., Kossin, J.P., Jagger, T.H., 2008. The increasing intensity of the strongest tropical cyclones. Nature 455, 92–95. https://doi.org/10.1038/nature07234

Emanuel, K., 2011. Global warming effects on U.S. hurricane damage. Weather. Clim. Soc. 3, 261--268. https://doi.org/10.1175/WCAS-D-11-00007.1

Federal emergency management agency (FEMA) -Mitigation division, 2014. Multi-hazard loss estimation methodology – hurricane model, Hazus–MH 2.1 Technical manual. Washington, D.C., USA.

Garciano, L.E., Hoshiya, M., Maruyama, O., 2005. Development of a regional map of extreme wind speeds in the Philippines. Struct. Eng. Eng. 22, 15–26. https://doi.org/10.2208/jsceseee.22.15s

Gentile, R., Galasso, C., Idris, Y., Rusydy, I., Meilianda, E., 2019. From rapid visual survey to multi-hazard risk prioritisation and numerical fragility of school buildings in Banda Aceh, Indonesia. Natural Hazards and Earth System Sciences Discussions, 19, 1365-1386.

Government of the Philippines, Republic Act No. 10066, 2009. National Cultural Heritage Act of 2009.

Grossi, P., Kunreuther, H., 2005. Catastrophe Modeling: A New Approach to Managing Risk.

Springer-Verlag, New York.

Henderson, D., Williams, C., Gavanski, E., Kopp, G.A., 2013. Failure mechanisms of roof sheathing under fluctuating wind loads. J. Wind Eng. Ind. Aerodyn. 114, 27–37. https://doi.org/10.1016/j.jweia.2013.01.002

Holden, W.N., Marshall, S.J., 2018. Climate change and typhoons in the Philippines: Extreme weather events in the anthropocene, in: Integrating Disaster Science and Management: Global Case Studies in Mitigation and Recovery. Elsevier Inc., pp. 407–421. https://doi.org/10.1016/B978-0-12-812056-9.00024-5

Iloilo City Cultural Heritage Conservation Council (ICCHCC), 2010. Implementing Rules and Regulations for the Downtown Central Business District (CBD) Heritage Zone. Iloilo City, Philippines.

Knutson, T.R., McBride, J.L., Chan, J., Emanuel, K., Holland, G., Landsea, C., Held, I., Kossin, J.P., Srivastava, A.K., Sugi, M., 2010. Tropical cyclones and climate change. Nat. Geosci. 3, 157--163. https://doi.org/10.1038/ngeo779

Konthesingha, K.M.C., Stewart, M.G., Ryan, P., Ginger, J., Henderson, D., 2015. Reliability based vulnerability modelling of metal-clad industrial buildings to extreme wind loading for cyclonic regions. J. Wind Eng. Ind. Aerodyn. 147, 176–85. https://doi.org/10.1016/j.jweia.2015.10.002

Lee, K.H., Rosowsky, D. V., 2005. Fragility assessment for roof sheathing failure in high wind regions. Eng. Struct. 27, 857–868. https://doi.org/10.1016/j.engstruct.2004.12.017

Mahendran, M. , Mahaarachchi, D. , 2002. Cyclic Pullout Strength of Screwed Connections in Steel Roof and Wall Cladding Systems using Thin Steel Battens. J. Struct. Eng. 128, 771–778. https://doi.org/10.1061/(ASCE)0733-9445(2002)128:6(771).

Masoomi, H., Ameri, M.R., Van De Lindt, J.W., 2018. Wind Performance Enhancement Strategies for Residential Wood-Frame Buildings. J. Perform. Constr. Facil. 32. https://doi.org/10.1061/(ASCE)CF.1943-5509.0001172

Mei, W., Xie, S.P., Primeau, F., Mc Williams, J.C., Pasquero, C., 2015. Northwestern Pacific typhoon intensity controlled by changes in ocean temperatures. Sci. Adv. 4, 1–8. https://doi.org/10.1126/sciadv.1500014

Moehle, J., Deierlein, G.G., 2004. A framework methodology for performance-based earthquake engineering, in: 13th World Conference on Earthquake Engineering. Vancouver, BC, Canada, pp. 3812–4.

Nguyen, M.N., Leicester, R.H., Wang, C.H., Foliente, G.C., 2013. Corrosion effects in the structural design of metal fasteners for timber construction. Struct. Infrastruct. Eng. 9, 275–284. https://doi.org/10.1080/15732479.2010.546416

Philippine Atmospheric Geophysical and Astronomical Services Administration (PAGASA),

2019. Climate of the Philippines [WWW Document]. URL http://bagong.pagasa.dost.gov.ph/information/climate-philippines

Philippine Statistics Autorithy, 2016. Census of Population 2015: “Region VI (Western Visayas)”. Total Population by Province, City, Municipality and Barangay. Report 2016-070.

Pita, G., Pinelli, J.P., Gurley, K., Mitrani-Reiser, J., 2015. State of the art of hurricane vulnerability estimation methods: A review. Nat. Hazards Rev. 16. https://doi.org/10.1061/(ASCE)NH.1527-6996.0000153

Qin, H., Stewart, M.G., 2019. System fragility analysis of roof cladding and trusses for Australian contemporary housing subjected to wind uplift. Struct. Saf. 79, 80–93. https://doi.org/10.1016/j.strusafe.2019.03.005

Rosić, B., Matthies, H.G., 2017. Sparse bayesian polynomial chaos approximations of elasto-plastic material models, in: XIV International Conference on Computational Plasticity. Fundamentals and Applications. Barcelona, pp. 256–267.

Saltelli, A., Chan, K., Scott, E.M., 2000. Sensitivity analysis. Wiley Series in Probability and Statistics, Wiley.

Sevieri, G., Andreini, M., De Falco, A., Matthies, H.G., 2019. Concrete gravity dams model parameters updating using static measurements. Eng. Struct. 196.

Sevieri, G., De Falco, A., 2020. Dynamic Structural Health Monitoring for concrete gravity dams based on the Bayesian inference. J. Civ. Struct. Heal. Monit. 380.

Sevieri, G., Galasso, C., D’Ayala, D., De Jesus, R., Oreta, A., Grio, M.E.D.A., Ibabao, R., 2020. A multi-hazard risk prioritization framework for cultural heritage assets. Nat. Hazards Earth Syst. Sci. 20, 1391–1414. https://doi.org/10.5194/nhess-20-1391-2020

Silang, A., Uy, S.N., Dado, J.M., Cruz, F.A., Narisma, G., Libatique, N., Tangonan, G., 2014. Wind Energy Projection for the Philippines Based on Climate Change Modeling. Energy Procedia 52, 26–37.

Silva, V., 2019. Uncertainty and correlation in seismic vulnerability functions of building classes. Earthquake Spectra, 35(4), 1515–1539.

Slamova, K., Glaser, R., Schill, C., Wiesmeier, S., Köhl, M., 2012. Mapping atmospheric corrosion in coastal regions: methods and results. J. Photonics Energy 2. https://doi.org/10.1117/1.jpe.2.022003

Sobol’, I.M., 1993. Sensitivity Estimates for Nonlinear Mathematical Models. Math. Model. Comput. Exp. 1, 407–414. https://doi.org/1061-7590/93/04407-008

Song, B., Galasso, C., Garciano, L., 2019. WARP^2: Wind Assessment of Roofs to Pullout & Pullover for Priority Cultural Heritage Structures in the Philippines, in: 13th International Conference on Applications of Statistics and Probability in Civil Engineering (ICASP13).

Seoul, South Korea.

Song, B., Galasso, C., Garciano, L., 2020. Wind-uplift fragility analysis of roof sheathing for cultural heritage assets in the Philippines. Int. J. Disast. Risk Re. 51, 101753.

Stewart, M.G., 2016. Climate change impact assessment of metal-clad buildings subject to extreme wind loading in non-cyclonic regions. Sustain. Resilient Infrastruct. 1, 32–45. https://doi.org/10.1080/23789689.2016.1181401

Stewart, M.G., Ginger, J.D., Henderson, D.J., Ryan, P.C., 2018. Fragility and climate impact assessment of contemporary housing roof sheeting failure due to extreme wind. Eng. Struct. 171, 464–475. https://doi.org/10.1016/j.engstruct.2018.05.125

Strobl, E., 2019. The impact of typhoons on economic activity in the Philippines: evidence from nightlight intensity (No. 589), ADB economics working paper series.

Sudret, B., 2008. Global sensitivity analysis using polynomial chaos expansions. Reliab. Eng. Syst. Saf. 93, 964–979.

United States Department of Agriculture (USDA), 2010. Wood Handbook. Wood as an Engineering Material. Madison, Wisconsin, USA.

Vecco, M., 2010. A definition of cultural heritage: From the tangible to the intangible. Journal of Cultural Heritage, 11(3), 321-324.

Vickery, P.J., Lin, J., Skerlj, P.F., Twisdale, L.A., Huang, K., 2006. HAZUS-MH hurricane model methodology. I: Hurricane hazard, terrain, and wind load modeling. Nat. Hazards Rev. 7, 82–93. https://doi.org/10.1061/(ASCE)1527-6988(2006)7:2(82)

Villarin, J.T., Algo, J.L., Cinco, T.A., Cruz, F.T., de Guzman, R.G., Hilario, F.D., Narisma, G.T., Ortiz, A.M., Siringan, F.P., Tibig, L. V., 2016. 2016 Philippine Climate Change Assessment (PhilCCA): The Physical Science Basis.

Xiu, D., 2010. Numerical Methods for Stochastic Computations. Princeton University Press.

Yang, Q., Gao, R., Bai, F., Li, T., Tamura, Y., 2018. Damage to buildings and structures due to recent devastating wind hazards in East Asia. Nat. Hazards 92, 1321--1353. https://doi.org/10.1007/s11069-018-3253-8